RoVaLL: Design and Development of a Multi-Terrain Towed Robot with Variable Lug-Length Wheels

Jose Salazar, Shin Matsuzaki and Yasuhisa Hirata[1]

***Abstract*—Robotic systems play a very important role in exploration, allowing us to reach places that would otherwise be unsafe or unreachable to humans, such as volcanic areas, disaster sites or unknown areas in other planets. As the area to be explored increases, so does the time it takes for robots to explore it. One approach to reduce the required time is using multiple autonomous robots to perform distributed exploration. However, this significantly increases the associated cost and the complexity of the exploration process.**

To address these issues, in the past we proposed a leader-follower architecture where multiple two-wheeled passive robots capable of steering only using brakes are pulled by a leader robot. By controlling their relative angle with respect to the leader, the followers could move in arbitrary formations. The proposed follower robots used rubber tires, which allowed it to perform well in rigid ground, but poorly in soft soil. One alternative is to use lugged wheels, which increase the traction in soft soils.

In this paper we propose a robot with shape-shifting wheels that allow it to steer in both rigid and soft soils. The wheels use a cam mechanism to push out and retract lugs stored on its inside. The shape of the wheel can be manipulated by controlling the driving torque exerted on the cam mechanism. Through experiments we verified that the developed mechanism allowed the follower robots to control their relative angle with respect to the leader in both rigid and soft soils.

***Index Terms*—Multi-Robot Systems; Mechanism Design; Wheeled Robots**

I. INTRODUCTION

IN many different situations, it's necessary to perform exploratory tasks over large areas. For example, Exploration Geophysics is an applied branch of geophysics that uses different physical methods on the earth's surface to measure properties of the subsurface, as well as anomalies. This is helpful for finding mineral resources such as fossil fuels or groundwater reservoirs, or even studying seismic activity. These activities are not only limited to the earth, but also in much more hostile environments such as the Moon or Mars. Another example where exploration is required is in the aftermath of disasters such as earthquakes or landslides. In order to quickly locating victims trapped under debris, it's necessary to scan the affected areas as effectively as possible.

Given the dangerous and precarious nature of these environments, researchers have proposed using robots to carry out the exploratory tasks more safely [1], [2]. Additionally, the exploration can be performed more efficiently by using multiple robots simultaneously [3]-[5].

Previously, we developed a towed two-wheeled robot for surface exploration which was able to steer using brakes attached to its rubber tires by a leader [6] or winch units [7]. By deploying multiple robots towed by a leader in formation, as shown in Fig. 1, we can perform simultaneous exploration of vast areas efficiently. Despite performing well in rigid surfaces, the robot was not able to adjust its position in soft or sandy surfaces. Circular rubber wheels can travel more efficiently in rigid ground because they have lower running resistance and provide less vibration on the robot's center of gravity . However, on soft ground, lugged wheels perform better as they can suppress sinking and slippage.

Therefore, in this research we propose the concept of a Robot with Variable Lug-Length wheels (RoVALL): a towed robot with wheels that can shape-shift into circular wheels or lugged wheels, and is able to change the wheel shape automatically according to the environment. This will enable the robot to efficiently traverse both soft and rigid grounds.

In the past, the concept of shape-shifting wheels for robots has been largely explored, although the main purpose is usually enabling the robot to have larger wheels or legged wheels in order to overcome obstacles and traverse around uneven terrain [8]-[16]. However, in our case, we propose pushing out lugs to generate more traction while traveling through soft terrain.

This paper has three main contributions: first, we propose a novel wheel that can change its shape from circular to lugged

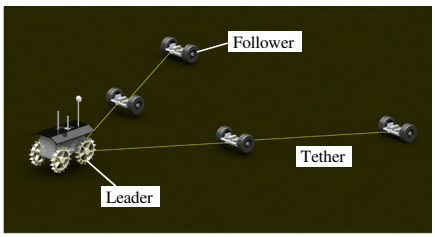

Fig. 1: Leader Follower Architecture using Multiple Mobile Robots [6]

Manuscript received: February, 24, 2020; Revised June, 18, 2020; Accepted July, 3, 2020.

This paper was recommended for publication by Editor Nak Young Chong upon evaluation of the Associate Editor and Reviewers comments.

This work was partially supported by JAXA's Space Exploration Innovation Hub Center.

[1]J. Salazar, S. Matsuzaki and Y. Hirata are with the Department of Robotics, Tohoku University, Sendai, Miyagi 980-8579, Japan j.salazar, s.matsuzaki, hirata@srd.mech.tohoku.ac.jp

Digital Object Identifier (DOI): see top of this page.

using a cam mechanism contained within itself. Second, we propose a control method that takes advantage of the difference in torque required to deploy the lugs in rigid and soft grounds, and uses this difference to apply steering force while deploying the lugs only on soft surfaces without requiring any sensors. Third, we propose a control method to adjust the robot's trajectory while being towed, based on the steering force.

II. VARIABLE LUG-LENGTH WHEEL MECHANISM

The proposed shape changing wheels with variable lug length is shown in Fig. 2. A grooved cam is built in the wheel, and the lugs move along the grooves based on the rotation of the cam. The length of the lug changes depending on the cam rotation angle. When the lugs are not deployed (left), it functions as a circular wheel, and when deployed, it functions as a lugged wheel (right).

As we explained before, the robot has no driving force and it's towed by a leader, and friction between the wheels and the ground causes the wheels to rotate. The direction of the cam grooves in each wheel is set so that in order to deploy the lugs, a torque that opposes the direction of rotation of the wheel (i.e., a braking torque) is required (indicated as the yellow arrow in Fig. 3(left)).

In this figure, the rotation direction of the wheel due to the robot being towed is clockwise, and the torque to deploy the lugs is applied in the counter-clockwise direction. Aside from producing the force to deploy the lugs (yellow arrow in Fig. 3 (right)), since the cam is arranged coaxially with the rotation axis of the wheel, the motor torque for rotating the cam generates a braking force opposed to the direction of motion through the wheel shell when it's in contact with the ground (red arrow in Fig. 3). In addition, if the torque is enough to deploy the lugs, a resistance force on the side of the lug is produced in the same direction, indicated by the green arrow. Since both the lug resistance and the braking force act in the opposite direction to the rotation direction of the wheels, the resultant force can be used for steering the robot, as different forces acting on the wheels would cause a difference in the rotational speed of the wheels, enabling the robot to steer. It's important to mention that even though there are two active DOF (rotation, lug deployment), both are achieved using a single motor, which makes the wheels underactuated.

The cam grooves' curve was designed according to Archimedes' spiral (Eq.(1)) so that the rotation angle and the amount of lug development were proportional. In this equation r is the radius of center to the spiral, a is a constant and θ is the angular position. The number of lugs of this prototype was decided based on the manufacturing feasibility and to maintain a certain amount of continuity when running on lugged wheels. As a result of these considerations, the robot developed in this paper is equipped with eight lugs. In future iterations, we will consider optimal spacing between lugs using existing literature [17].

$$r = a\theta \tag{1}$$

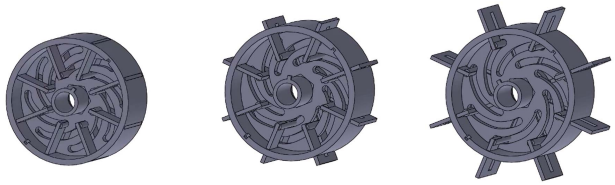

Fig. 2: Extension of Lug by Cam Mechanism

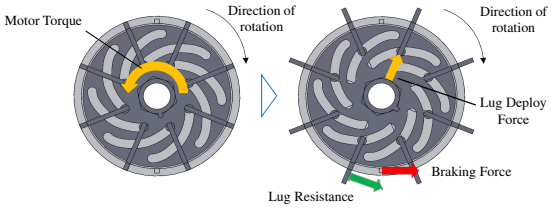

Fig. 3: Steering Force by Lugs and Brake

A. Lug Deployment Conditions

In this section, we consider the forces acting on the lugs and cam, and derive the motor torque required for the lugs to unfold. Using this, it is possible to select the required motor and control the voltage applied to the motor appropriately.

First, we consider the balance of forces acting on the lug. Fig. 4(a) shows the side view of the wheel and the force acting on the lug. Here we consider the situation where the lug is positioned perpendicularly to the ground, so the resistance F_G from the ground is acting perpendicularly to the lug. This is the case where normal force is largest so it's the most difficult position to expand the lugs. From this situation we can obtain the maximum required motor torque. In addition to the lug, the normal drag F_S and frictional force μF_S from the outer shell of the wheel, and the normal drag F_C and friction from the cam μF_C are acting. Considering the balance of these forces in the x-axis and y-axis directions, Eq.(2) is given.

$$\begin{cases} F_S = F_C \sin\phi + \mu F_C \cos\phi \\ F_G + \mu F_S = F_C \cos\phi - \mu F_C \sin\phi \end{cases} \tag{2}$$

From the above equation, F_C, which is the normal drag that the lug receives from the cam, is obtained as follows.

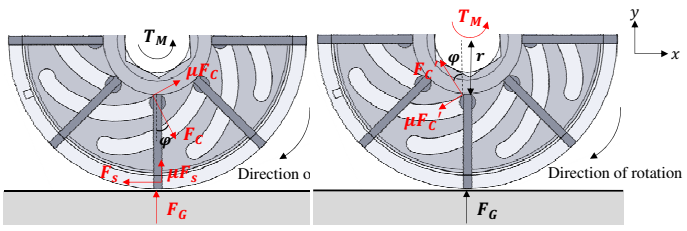

(a) Lug (b) Cam

Fig. 4: Dynamics of the Wheel

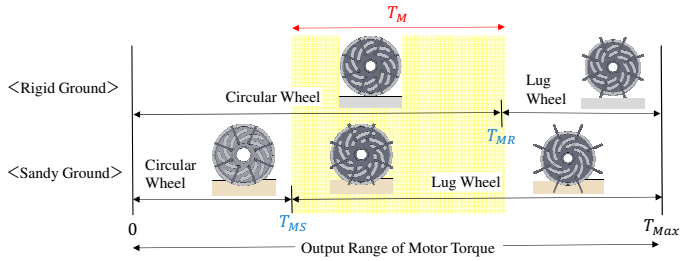

Fig. 5: Relationship between Motor Torque and Wheel Form

$$F_C = \frac{F_G}{(1-\mu^2) - 2\mu \sin\phi} \tag{3}$$

Next, consider the balance of the torque acting on the cam. Fig. 4 (b) shows the forces acting on the cam. The reaction force of F_C, F'_C, its frictional force $\mu F'_C$, and motor torque F_M act on the cam. Since F'_C is a reaction of F_C, it can be expressed as (4).

$$F'_C = -F_C \tag{4}$$

Here, the equation (5) is given considering the balance of the torque acting on the cam.

$$T_M = (F_C \sin\phi + \mu F_C \cos\phi) \times r \tag{5}$$

From the expressions 3, 4, and 5, the condition of the motor torque required for the unfolding the lug is obtained using Eq. (6).

$$T_M \geq \frac{r F_G (\sin\phi + \mu \cos\phi)}{(1-\mu^2) - 2\mu \sin\phi} \tag{6}$$

From the above equation, it can be seen that T_M is a value proportional to F_G. In other words, the greater the normal force, the more difficult it is for the lug to unfold, and a greater motor torque is required. In addition, the normal force gradually decreases as it's applied at an angle when the wheel rotates, and would become zero when the lug moves away from the ground. However, in the developed wheel mechanism, since all eight lugs are connected to a single cam, T_M does not become 0 as long as the ground exerts a force in one of the lugs.

The lug expansion condition obtained in Eq.(6) depends on the normal force applied from the ground. Here, the magnitude of the normal force differs between solid ground and soft ground, and is considered to be a value that depends on the driving environment. In other words, the conditions to deploy the lugs depends on the driving environment. In this study, two environments are assumed: a solid ground and a soft ground. These conditions and the corresponding possible wheel shapes are considered in the next section.

B. Wheel Shape-shift due to Driving Environment

In this section, we consider the possible wheel shapes of the designed variable lug-length wheel in two environments, solid ground and soft ground. Fig. 5 shows a conceptual diagram showing the relationship between output motor torque and wheel shape in each driving environment. Here, the horizontal axis represents the output range of the motor torque. In addition, T_{MR} is the required torque for extending the lugs on solid ground, and T_{MS} is the torque required for extending the lugs on soft ground. First, considering the solid ground, when the motor torque is less than T_{MR}, the lugs run on circular wheels without expanding. During this time, lugs are not deployed, but the motor torque is converted to braking force only, so that steering the robot is performed only using the braking force, as proposed in our previous research. Then, when the motor torque exceeds T_{MR}, the lugs are deployed and the vehicle runs using the lugged wheels. Next, when considering soft ground, it is considered that the vehicle runs with circular wheels when the motor torque is less than T_{MS}, and when it is more than T_{MS}, the wheels transform into lugged wheels.

Here, when traveling on soft ground, the contact area between the wheels and the ground increases, so that the contact pressure decreases and the normal force acting on the lugs decreases. As a result, the relation in Eq. (7) is obtained, and we observe that the the torque required to deploy the lugs on soft ground is lower than on solid ground.

$$T_{MS} < T_{MR} \tag{7}$$

According to Eq. (7), there is a gap or difference in the torque required to deploy the lugs between solid ground and soft ground. Taking advantage of this, by controlling the motor torque T_M within the output range of $T_{MS} < T_M < T_{MR}$, the system will operate using circular wheels on solid ground, as the torque is not enough to push the lugs out, but it will be able to deploy its lugs in soft ground, as the torque will be enough to push them out in a soft ground. This enables the robot to change its wheels shape without requiring any additional sensors to determine the type of ground. We'd like to remark that the robot cannot determine the type of ground it's running, but the lugs are rather able or not able to be deployed depending on the surface, as the applied torque is kept within the specified range.

C. Steering Method

In this section we describe the steering control method. As stated before, the braking elements are lug resistance and braking force. We call the sum of these forces the steering force. This method is derived from our previous work [6], with the additional term of lug resistance.

Fig. 6 is a diagram showing the process of the robot turning by generating steering force while being towed. First, at time t_0, the robot is located at tether angle $\theta = 0$ [deg] with respect to the leader. We set the desired tether angle as θ_{des}, considered turning to the left with respect to the advancing direction as can be seen in Fig. 6. The target steering angle

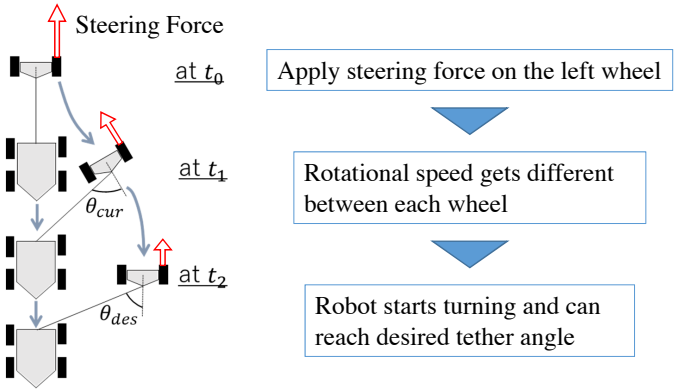

Fig. 6: Steering the Robot by Lug Resistance and Brake Force

can be reached by applying a larger steering force (sum of braking force and lug resistance) to the wheel in the direction in which the follower needs to turn. In the case of Fig. 6, the steering force is applied to the left wheel of the follower. At this time, the rotation speed of the left wheel is lower than that of the right wheel due to the steering force. As a result, the robot gradually turns to the left due to the difference in rotational speed. An arbitrary tether angle can be maintained by measuring the current tether angle θ_{cur} and controlling the motor torque appropriately. Even when multiple followers are used, each robot is controlled independently. By setting the target tether angle of each robot, we can achieve arbitrary formations without knowing each others' position. Furthermore, it is desirable that the steering force applied to the wheel is as small as possible. This is because in a leader-follower system, an active leader pulls the follower robots, and if more steering force than necessary is generated, a larger tractive force is required and the burden on the leader increases. In other words, the smaller the steering force acting on the wheels, the more energy can be saved in the entire system.

III. STRUCTURE OF ROVALL

A. System Architecture

In this section, we introduce the developed Robot with Variable Lug-Length wheels (RoVALL), which can be towed as a follower in the leader-follower architecture proposed by the authors in the past. The appearance of RoVALL is shown in Fig. 7. RoVALL uses the lug resistance force and the braking force to steer itself using the difference in rotational speed between the wheels. To simplify the control, we implemented RoVALL as an opposed two-wheel type robot, using the proposed variable lug-length wheels. A passive wheeled stabilizer is installed at the rear to allow the RoVALL to drive in a more straight manner. A motor to drive the cam is attached to each wheel. As we require a torque of 0.18 [Nm] or more, we chose a motor with a stall torque of 0.28 [Nm].

Fig. 8 shows an actual RoVALL unit. Main specifications are shown in Tab. I. Most of the fuselage and wheels were 3D printed in ABS. The lugs were made of acrylic, and the motor applied the torque to the wheel through gears, as can be seen in Fig. 9. The RoVALL is equipped with a potentiometer

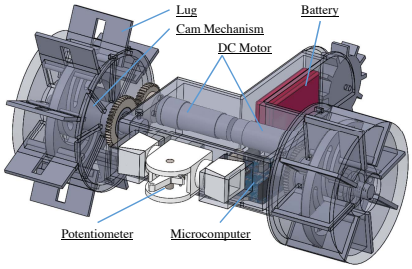

Fig. 7: Design View of RoVALL

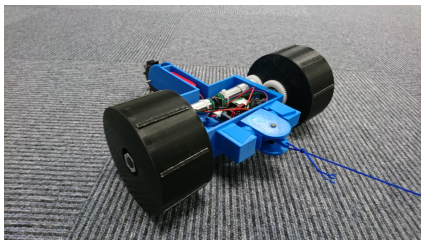

Fig. 8: Developed RoVALL

unit that measures the tether angle in order to determine the relative position of RoVALL with respect to the leader. The tether is connected to a two-axis gimbal mechanism (Fig. 10), which allows the proper tether angle to be measured even when the RoVALL is tilted up or down due to unevenness on the ground. We used a Raspberry Pi 3 Model B to control the left and right motors and read the potentiometer. The system is implemented on ROS. As a result, it is possible to wirelessly acquire tether angle data and transmit command values such as target tether angle. In addition, a 5V / 2.4A output battery is provided to supply power to the Raspberry Pi.

TABLE I: Main Specification of RoVALL

Features	Values
Mass	970 [g]
Size(Length×Width×Height)	296×278×110 [mm]
Radius of the Front Wheels	55 - 75 [mm]
Width of the Front Wheels	58 [mm]
Radius of the Rear Wheel	24 [mm]
Width of the Rear Wheel	13.5 [mm]

B. RoVALL Control

This section describes the control system for following an arbitrary tether angle. The geometric relationship between the leader and the follower RoVALL is shown in Fig. 11. The desired tether angle is θ_{des}, the current tether angle is θ_{cur}, and their difference is $\Delta\theta$. We create a smooth target tether angle trajectory using a fifth-order polynomial interpolation. In order to follow the target value, the motor torque is calculated using a PID controller, described in Eq.(8). Here, K_p, K_d, and K_i are feedback gains.

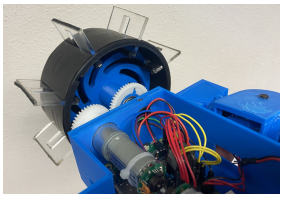

Fig. 9: Wheel Detail

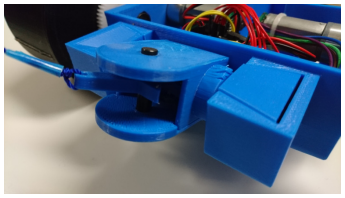

Fig. 10: Potentiometer Unit

Fig. 12: Pressure Sensor "FSR400"[19]

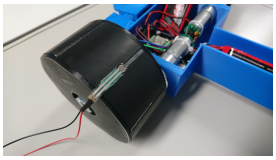

Fig. 13: Sensor Arrangement

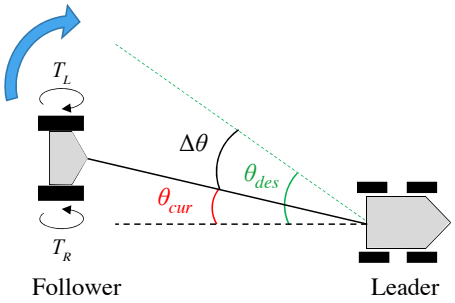

Fig. 11: Steering Control for Follower Robot

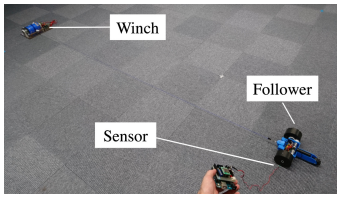

Fig. 14: Experimental Environment

$$T_L = \begin{cases} K_p\Delta\theta + K_d\Delta\dot{\theta} + K_i\int\Delta\theta dt & (\theta_{des} \geq 0) \\ T_{MS} & (\theta_{des} < 0) \end{cases}$$
$$T_R = \begin{cases} T_{MS} & (\theta_{des} > 0) \\ K_p\Delta\theta + K_d\Delta\dot{\theta} + K_i\int\Delta\theta dt & (\theta_{des} \leq 0) \end{cases} \quad (8)$$

$where:$

$$T_L = \begin{cases} T_{MS} & (T_L < T_{MS}) \\ T_{MR} & (T_L > T_{MR}) \end{cases}$$
$$T_R = \begin{cases} T_{MS} & (T_R < T_{MS}) \\ T_{MR} & (T_R > T_{MR}) \end{cases}$$

The upper limit is set to be T_{MR} and the lower limit is set to T_{MS} to enable the aforementioned sensorless shape-shifting of the wheel. In addition, in order to minimize the amount of steering, the lower limit T_{MS} always acts on the wheel in the direction opposite to the turning direction. The reason why the motor torque is not set to zero is for the robot to deploy the minimum lug length in soft ground and to keep the tether tension constant. As some steering force is constantly applied, we can expect the tether to be kept in tension.

C. Normal Force Measurement

In order to determine the output range of the motor torque, it is necessary to determine the lug deployment condition, which depends on the normal force F_G as can be seen in Eq. (6). In this section, we measure the normal force acting on the lug. By determining the required output range of the motor torque, we can select the motor and establish our control mechanism.

Keio University has been conducting research on analyzing the stress state of a wheel using a wheel with a built-in pressure sensor[18]. Similarly, we measured the normal force using a Interlink Electronics FSR400 (Fig. 12 [19]) pressure sensor in order to obtain the lug deployment condition T_{MR} on the solid ground. We attached the sensor to the lug as shown in Fig. 13, and measured on a solid ground. An external view of the experimental environment is shown in Fig. 14. The solid ground used in this study is a polypropylene cut pile carpet in our laboratory shown in Fig. 14. Here, the follower is pulled by a winch. The winch can be wound at any speed. To measure the vertical drag in this experiment, the winding speed was set to 300 [mm/s].

As a result, the graph shown in Fig. 15 was obtained. First, we can observe periodic peaks according to the rotation of the wheel. The average value of these peaks was found to be about 2.18 [N], with a standard error of 0.303 [N]. Tab. II shows the other parameters required to derive T_{MR}. Substituting the measured values into Eq. (6), we found T_{MR} = 0.18 [Nm]. From this, by selecting a motor and gearbox that can generate a torque slightly larger than 0.18 [Nm] and controlling the motor in the range of 0.18 [Nm] or less, we can control the robot in both rigid and soft grounds as explained before. Although it's also necessary to determine the lower limit T_{MS} on soft ground, this was no trivial task, so we set this value empirically from experimental results.

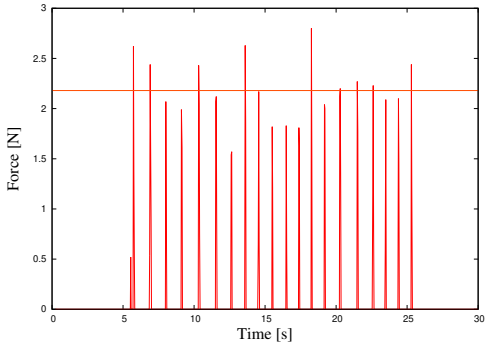

Fig. 15: Measured Force

TABLE II: Values of Parameters

Parameter	Value
Radius of the Cam r	20.6 [mm]
Angle ϕ	37 [deg]
Coefficient of Friction μ (ABS)	0.38

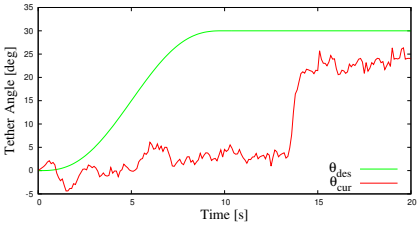

Fig. 16: Tether Angle Transition using Lug Wheel on Rigid Ground

IV. STEERING CONTROL EXPERIMENTS

In this section, we verified the feasibility of the proposed steering control method, both in rigid and soft grounds. In each experiment, only one RoVALL follower is towed using a winch.

A. Steering Verification in Rigid Ground

This section examines the steering performance of the follower on rigid ground, and whether the proposed method allowed the RoVALL to steer without deploying the lugs. Two conditions were set for the wheel shape: (1) running on lugged wheels, by locking the lugs of the RoVALL in the deployed state. In this case, the steering force comes only from the drag force of the lug in contact with the floor. The second condition is (2) running on circular wheels using the proposed control method. The target tether angle was 30 [deg]. The follower was towed using a winch as a substitute for the leader, with a winding speed of 500 [mm/s]. This procedure was repeated 5 times for each condition.

Fig. 16 shows the tether angle when the RoVALL ran on rigid ground with the deployed lugs. Fig. 17 shows the tether angle when the RoVALL travelled on rigid ground with circular wheels using the proposed control method.

From these experiments, we observed that when the vehicle traveled on solid ground with lugged wheels, the wheels did not rotate and were dragged due to slip. At some point beyond 10 [s], the lugs finally provided enough traction to allow the wheel to rotate, but the RoVALL did not reach the target tether angle. Opposedly, from Fig. 17, we can observe that it was possible to follow the target tether angle using the proposed control method. In these experiments, we observed that the lugs were not deployed and the RoVALL wheels were in the circular shape.

B. Steering Verification in Soft Ground

In this experiment, we verified RoVALL's steering performance on soft ground. The experiment was performed on a sandy ground with a particle size of about 0.5 [mm] to 0.25 [mm]. Two similar conditions were set for the RoVALL: (1) the lug extension mechanism was fixed so that the lugs were not deployed and the vehicle traveled using circular wheels, and (2) the vehicle traveled using the lugged wheels controlled using the proposed method. Similarly to the experiment in the previous section, the RoVALL was towed using a winch at a winding speed of 500 [mm / s], and the target tether angle was set to -30 [deg]. This procedure was repeated 5 times for each condition.

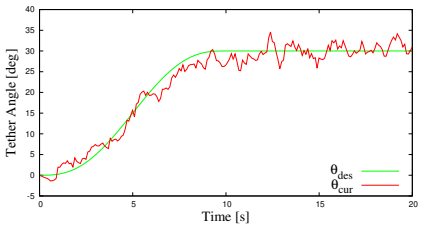

Fig. 17: Tether Angle Transition using Circular Wheel on Rigid Ground

Fig. 18 shows the change of the tether angle through time when traveling on soft ground with circular wheels. Fig. 19 shows the tether angle's change in time when running on lugged wheels on soft ground, using the proposed control method.

From Fig. 18, we can observe that the robot was not able to reach the target tether angle using circular wheels. In these experiments, we observed that the circular wheel did not get enough traction from the sandy ground, which is consistent with the results obtained in our previous research. On the other hand, in Fig. 19 we can observe that when the lugs were deployed, the RoVALL was able to reach the target tether angle. However, we found that the oscillation of the tether angle was larger than that of traveling on rigid ground. This is mainly caused because of the irregularities and unevenness of the ground, which slightly change the pose of the RoVALL while advancing, which in turn affects the measurements of the potentiometer. However, the general position of the robot did not change much. From this, we evidenced that the robot was able to deploy the lugs and reach the desired angle correspondingly.

Furthermore, in this experiment, since the follower made a right turn, the lug of the right wheel should have expanded more than the left wheel. In Fig. 20 we can see an enlarged view of the follower's tracks immediately after the experiment. We can confirm from the appearance of the wheels and the tracks that the lugs of the right wheel were expanded significantly more than the left wheel. From the above, we verified that by appropriately controlling the left and right motor torques, it is possible to adjust the amount of lug deployed and control the steering towards the desired angle.

V. FORMATION CONTROL EXPERIMENTS

In this section, we perform a formation control experiment using three robots. The desired formation is shown in Fig. 21. Two RoVALL units are towed by a leader robot, and the desired angles are set so the robots move in a V-shaped arrangement.

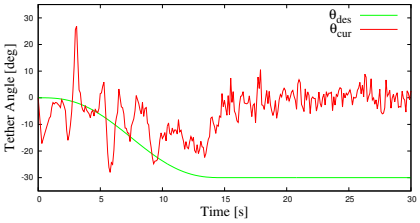

Fig. 18: Tether Angle Transition using Circular Wheel on Soft Ground

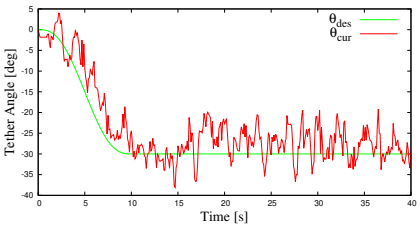

Fig. 19: Tether Angle Transition using Lug Wheel on Soft Ground

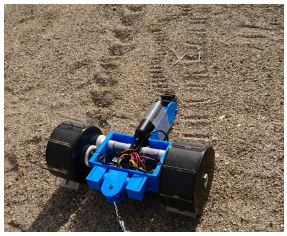

Fig. 20: Tether Angle Transition on Rigid Ground

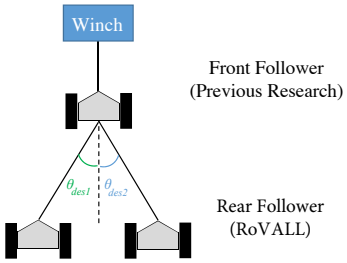

Fig. 21: V-Shaped Formation

A. Formation Control in Rigid Ground

For this experiment, we used an unit developed in previous research [6] on the front towing two RoVALL units attached to it. As desired tether angles, 0 [deg] was given to the leading robot, and 30 [deg] and -30 [deg] were given to RoVALL units in the back. The winding speed of the winch was 500 [mm / s].

Fig. 22 shows the change in time of the tether angle from the two RoVALL units in the back. Fig.23 shows a freeze-frame sequence from the experiment, taken every 5 [s].

We can evidence that each RoVALL unit was able to control its steering angle and reach to the target value . In Fig. 23 we can observe that the V-shaped formation was gradually reached.

B. Formation Control in Soft Ground

In this section, we performed a similar experiment to the previous one , but on soft ground. The robot on the front was replaced for one with lugged wheels developed on previous research [6]. The desired angles were the same.

The change in time of the tether angle for each RoVALL unit are shown in Fig. 24. Fig.25 shows a freeze-frame sequence of the experiment, taken every 5 [s].

From Fig. 24, we observed that the two followers reach their respective target angles on sandy ground. From Fig. 25, we can similarly observe that the formation was eventually reached.

VI. DISCUSSION

In Section 4, we verified through experiments that the developed RoVALL units can be used on both rigid and soft grounds. We observed that desired tether angles were reachable by using the proposed control method, and we verified its feasibility by achieving a specific formation using multiple followers. Although we did not observe any jamming issues, we could observe that some sand would enter the wheels after some experimental runs. We will consider ways to mitigate this in future iterations.

However, despite both formations reaching the same desired angle, in Fig. 23(e) and Fig. 25(h) we can see there's a difference in the final state of the formation, particularly in the distance between the two robots, in rigid and soft ground, respectively. Despite the tether angles (Fig. 22, 24) converging to the same target value, this difference in distance is caused by the follower's attitude. On solid ground, the vehicle runs in a straight manner, aligned with the direction of travel. On the other hand, on soft ground, the vehicle seems to be running at an angle facing outwards the actual traveling direction. This might occur because the lugged wheels developed in this study could not completely suppress slippage on sandy ground, and skidding occurred. As a result, the tether angle was properly controlled, but the follower position with respect to the global frame of reference was different. This leads to a decrease in exploratory performance, so in order to obtain a deployment range similar to solid ground, it is necessary to improve hardware or software to further suppress skidding, or consider measuring the robot's position in the global frame of reference.

VII. CONCLUSIONS

In this paper we proposed a towed Robot with Variable Lug-Length wheels (RoVALL) that is able to adjust its position when being towed in both rigid and soft soils. The robot's wheels contain a cam mechanism to push out and retract lugs stored on its inside. The shape of the wheel can be manipulated by controlling the torque of a motor exerted on the wheel. Through experiments we verified that the developed mechanism allowed the follower RoVALL units to control their relative angle with respect to the leader in both rigid and soft soils. Although the proposed RoVALL was able to reach the desired tether angles, there are still some obstacles

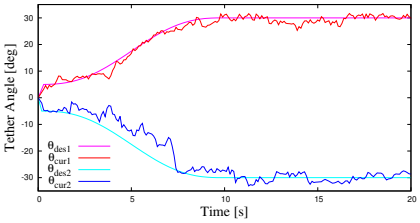

Fig. 22: Tether Angle Transition on Rigid Ground

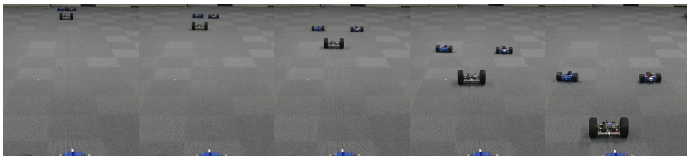

(a) 0 [sec] (b) 5 [sec] (c) 10 [sec] (d) 15 [sec] (e) 20 [sec]

Fig. 23: V-shaped Formation on Rigid Ground

remaining, such as its inability to entirely suppress skidding when traversing through soft ground. In order for the system to perform accordingly, it is necessary to improve hardware to withstand the lateral component of the tether tension. Additionally, when considering the use on uneven terrain, the tether may come into contact with obstacles, etc., and the formation control may be disrupted or disconnected. As a method to solve this problem, we could extend the tether from above using a crane or the like as a leader in order to provide clearance with the ground. In the future we want to measure the accuracy of the system in reaching arbitrary positions by measuring its position in the global frame of reference. Additionally, we'd like to apply the proposed system to exploration activities and verify its effectiveness compared with commonly used solutions for both rigid and soft surfaces.

REFERENCES

[1] "Aiming to Probe for Buried Vehicles Using a Drone After Landslides", https://www.aist.go.jp/aist-e/list/latest-research/2018/20180601/en20180601.html accessed at 28. August. 2019.

[2] K. Nagatani et al.,"Volcanic ash observation in active volcano areas using teleoperated mobile robots - Introduction to our robotic-volcano-observation project and field experiments," 2013 IEEE International Symposium on Safety, Security, and Rescue Robotics (SSRR), Linkoping, 2013, pp. 1-6.

[3] J. Luo, C. Liu and F. Liu, "A leader-following formation control of multiple mobile robots with obstacle," 2015 IEEE International Conference on Information and Automation, Lijiang, 2015, pp. 2153-2158.

[4] T. Fong, S. Grange, C. Thorpe and C. Baur, "Multi-robot remote driving with collaborative control," 10th IEEE International Workshop on Robot and Human Interactive Communication (ROMAN), Bordeaux, Paris, France, 2001, pp. 237-242.

[5] H. Beglerovic, Y. Hirata and K. Kosuge, "Formation control of multiple passive type boats for sea surveillance," 2016 IEEE/SICE International Symposium on System Integration (SII), Sapporo, 2016, pp. 869-874.

[6] Y. Hirata, K. Kimura, S. Matsuzaki, N. Ogawa, and T. Kubota, "Control of Multiple Passive-Follower Type Robots Based on Feasible Braking Control Region Analysis" 2018 IEEE International Conference on Robotics and Automation (ICRA), 2018.

[7] J. V. Salazar L., M. Hoshi and Y. Hirata, "Wide Area Exploration System Using Passive-Follower Robots Towed by Multiple Winches" 2020 IEEE/RSJ International Conference on Intelligent Robots and Systems (IROS), 2020 (to appear).

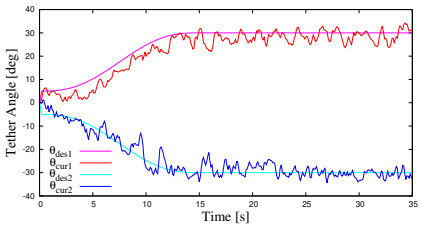

Fig. 24: Tether Angle Transition on Soft Ground

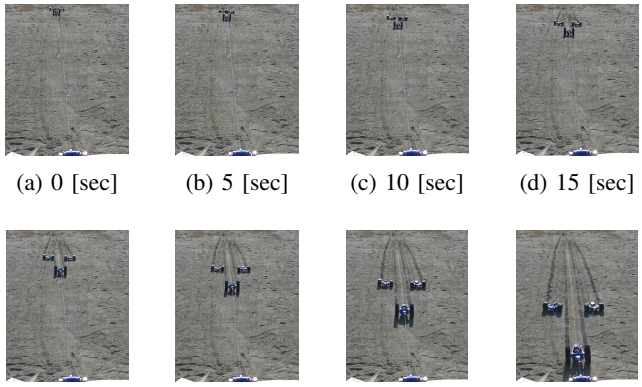

(a) 0 [sec] (b) 5 [sec] (c) 10 [sec] (d) 15 [sec]

(e) 20 [sec] (f) 25 [sec] (g) 30 [sec] (h) 35 [sec]

Fig. 25: V-shaped Formation on Soft Ground

[8] J. B. Jeans and D. Hong, "IMPASS: Intelligent Mobility Platform with Active Spoke System," 2009 IEEE International Conference on Robotics and Automation (ICRA), Kobe, 2009, pp. 1605-1606.

[9] X. Chen, F. Gao, Z. Wang, S. Yao, G. Xu and X. Yao, "Mechanism Principle and Dynamics Simulation on Variable Diameter Walking Wheel," Second International Conference on Digital Manufacturing & Automation, Zhangjiajie, Hunan, 2011, pp. 723-727.

[10] J. Koh, D. Lee, S. Kim and K. Cho, "Deformable soft wheel robot using hybrid actuation," 2012 IEEE/RSJ International Conference on Intelligent Robots and Systems (IROS), Vilamoura, 2012, pp. 3869-3870.

[11] S. M. Felton, D. Lee, K. Cho and R. J. Wood, "A passive, origami-inspired, continuously variable transmission," 2014 IEEE International Conference on Robotics and Automation (ICRA), Hong Kong, 2014, pp. 2913-2918.

[12] S. Chen, K. Huang, W. Chen, S. Shen, C. Li and P. Lin, "Quattroped: A Leg–Wheel Transformable Robot," in IEEE/ASME Transactions on Mechatronics, vol. 19, no. 2, pp. 730-742, April 2014.

[13] W. Chen, H. Lin, Y. Lin and P. Lin, "TurboQuad: A Novel Leg-Wheel Transformable Robot With Smooth and Fast Behavioral Transitions," in IEEE Transactions on Robotics, vol. 33, no. 5, pp. 1025-1040, Oct. 2017.

[14] Lan Zheng, Peng Zhang, Ying Hu, Gang Yu, Zhangjun Song and Jianwei Zhang, "A novel high adaptability out-door mobile robot with diameter-variable wheels," 2011 IEEE International Conference on Information and Automation, Shenzhen, 2011, pp. 169-174.

[15] Y. Kim, G. Jung, H. Kim, K. Cho and C. Chu, "Wheel Transformer: A Wheel-Leg Hybrid Robot With Passive Transformable Wheels," in IEEE Transactions on Robotics, vol. 30, no. 6, pp. 1487-1498, Dec. 2014.

[16] Yu She, C. J. Hurd and H. Su, "A transformable wheel robot with a passive leg," 2015 IEEE/RSJ International Conference on Intelligent Robots and Systems (IROS), Hamburg, 2015, pp. 4165-4170.

[17] K. Skonieczny, S. J. Moreland and D. S. Wettergreen, "A grouser spacing equation for determining appropriate geometry of planetary rover wheels," 2012 IEEE/RSJ International Conference on Intelligent Robots and Systems (IROS), Vilamoura, 2012, pp. 5065-5070.

[18] T. Shirai, G. Ishigami, "Development of in-wheel sensor system for accurate measurement of wheel terrain interaction characteristics" in Journal of Terramechanics, Vol.62, pp.51-61, 2015.

[19] Interlink Electronics "FSR400", available at https://www.interlinkelectronics.com/fsr-400